A simple classical model for predicting onset crystallization temperatures on curved substrates and its implications for phase transitions in confined volumes

Sharon J. Cooper,[a] Catherine E. Nicholson, and Jian Liu
Chemistry Department, Science Laboratories, Durham University, South Road, Durham DH1 3LE, United Kingdom

(Received 1 February 2008; accepted 14 August 2008; published online 30 September 2008)

For small confinement volumes, phase transition temperatures are determined by the scarcity of the crystallizing material, rather than the magnitude of the energy barrier, as the supply of molecules undergoing the phase transition can be depleted before a stable nucleus is attained. We show this for the case of crystallization from the melt and from the solution by using a simple model based on an extended classical nucleation theory. This has important implications because it enables a simple and direct measurement of the critical nucleus size in crystallization. It also highlights that predicting the observable melting points of nanoparticles by using the Gibbs–Thomson equation can lead to substantial errors. © *2008 American Institute of Physics*. [DOI: 10.1063/1.2977993]

I. INTRODUCTION

The crystallization and melting temperatures of materials in confined volumes can vary extensively from those observed in the bulk phases. Hence it is important that theories are derived to model these cases, particularly as the findings are pertinent to a diverse range of areas including nanomaterial production, rock weathering, and oil recovery. The rate of crystallization at a particular temperature is generally determined by the size of the energy barrier to the creation of the new phase. The same is not necessarily true for crystallization in nanosystems, however, because the supply of crystallizable molecules can be depleted before the process becomes energetically feasible. For instance, in Fig. 1, the system may have enough energy to attain the critical nucleus size r^*, but there may be insufficient material for the nucleus to grow to a size r_0. In this paper, we show the validity of this premise by using a simple phenomenological model based on an extended classical nucleation theory (CNT). Furthermore, when the crystallization temperature is limited by the availability of crystallizing material, we find that the critical nucleus size can then be found directly from the confinement size. Thus, there is no reliance on the Gibbs–Thomson equation and the application of bulk interfacial tension and enthalpy of fusion values to the tiny critical nucleus. We have recently used this approach to provide the first direct measurement of the critical nucleus size for ice crystallization in microemulsions.[1]

For most substances, surface melting occurs at a lower temperature than the bulk, and hence bulk melting occurs by thickening of this layer without the need for superheating above the equilibrium melting temperature T_{eq}. For small particles, this results in melting below the equilibrium melting temperature, with the melting point depression ΔT_m often modeled[2,3] by the Gibbs–Thomson equation,

$$\Delta T_m = T_{eq} - T_m = (2\gamma v_l T_{eq})/R\Delta_{fus}H, \tag{1}$$

where T_m is the melting temperature, γ is the melt-crystal interfacial tension, v_l is the liquid molecular volume, R is the particle radius, and $\Delta_{fus}H$ is the enthalpy of fusion.

Theoretical treatments have shown,[4–6] however, that the Gibbs–Thomson equation actually represents to the first approximation[7] the upper bound for melting of small solid particles when a surface liquid layer is present. This is because the Gibbs–Thomson equation gives the condition for the unstable equilibrium between the solid particle and the melt, and so represents the melting transformation pathway for which the energy barrier is zero. The thermal energy available to surmount energy barriers would then be expected to allow melting of the particle below this temperature, i.e., the *observable* melting temperature is below that given by the Gibbs–Thomson equation.[8]

A lower bound of the melting point has also been derived,[9] based on the criterion that the melting of the particle must be energetically feasible, i.e., the change in the free energy must be ≤ 0. This criterion is satisfied when

$$\Delta T_m = (3\gamma v_l T_{eq})/R\Delta_{fus}H. \tag{2}$$

Hence

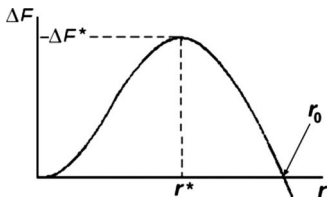

FIG. 1. Example graph of the Helmholtz free energy of formation ΔF of a nucleus of radius, r. The ΔF^*, r^*, and r_0 values are shown.

[a]Electronic mail: sharon.cooper@durham.ac.uk.

$$T_{\mathrm{eq}}\left[1-\frac{3\gamma v_l}{R\Delta_{\mathrm{fus}}H}\right]\leq T_m\leq T_{\mathrm{eq}}\left[1-\frac{2\gamma v_l}{R\Delta_{\mathrm{fus}}H}\right]. \quad (3)$$

For crystallization, the (typical) absence of a pre-existing solid surface layer means that the phase transformation must normally occur via the formation of a stable nucleus, which then grows to become the new bulk phase. The energy barrier to the creation of the stable nucleus leads to supercooling before the new phase appears. The size of the nucleation energy barrier can be modeled using CNT, first developed by Volmer and Weber,[10] and Becker and Döring.[11]

There have been many modifications to CNT to improve its validity, though mostly for the case of liquid condensation from the vapor.[12] Although a general theory applicable to a wide range of systems has not emerged, it is recognized that CNT is most applicable to systems at low supersaturation, where the critical nucleus size is correspondingly larger. This minimizes inaccuracies due to the assignment of macroscopic thermodynamic properties to the critical nucleus and in predicting its correct degrees of freedom. The development of nucleation theorem,[13–15] originally in connection with CNT, has been particularly insightful, since for *isothermal* crystallization experiments the number of molecules n^* in the critical nucleus can be reliably estimated from $n^*=(\partial(kT\ln J)/\partial\Delta\mu)_{V,T}$, where J is the nucleation rate and $\Delta\mu$ is the supersaturation. When the experimental variable is temperature, however, as is commonly the case for melt crystallization, the excess entropy of the critical nucleus also has to be considered. In this case, a direct evaluation of n^* from the variation of J with $\Delta\mu$ is no longer possible.[14]

Theoretical studies of nucleation using kinetic theories[12,16] and density functional theory[17–19] have also emerged to circumvent the problems associated with using CNT at high supersaturations and the assumption of a sharp interface between the parent and daughter phases. These, combined with simulations[20–23] of nucleation, are providing ever greater insight into the nucleation process. Despite these advances, the effect of confinement on the nucleation barrier has been much less studied.[4–6] We will show in this paper that consideration of this allows reliable critical nucleus sizes to be determined from *nonisothermal* crystallization experiments.

In this study, we derive onset crystallization temperatures for heterogeneous and homogeneous nucleations in confined volumes and so the following results are particularly relevant. Classical heterogeneous nucleation theory has been extended to account for nucleation upon *convex* substrates.[24–26] We now broaden this work to nucleation upon *concave* substrates and relate the nucleation free energy barrier for flat and curved substrates to obtain onset crystallization and melting temperatures applicable in any confined system within the limitations of our simple model. Models for nucleation in confined volumes have been derived previously. In particular, the effect on the supersaturation caused by the Laplace pressure difference across a curved surface has been considered by Kashchiev and van Rosmalen.[27] Hartman showed[28] that in confined systems, a stable minimum can occur at larger nucleus sizes than that of the critical nucleus owing to depletion of the supersaturation as the nucleus grows. In the extended modified liquid drop (EMDL) model, Reguera *et al.*[8] used a capillarity approach for the case of homogeneous nucleation of a liquid from the vapor in confined volumes and also found a free energy minimum at larger nucleus sizes. Their EMDL theory has since been developed[29] to include dynamical nucleation theory,[30] so that the spinodal could be reproduced. Shirinyan and Wautelet[31] considered the depletion of the nucleating phase for phase transitions in binary composition nanosystems. In their treatment, homogeneous nucleation is assumed and a regular solution model is adopted, with results pertinent to phase separation in alloys presented. The studies of Reguerra *et al.*[8,29] and Shirinyan and Wautelet[31] both identified for isothermal crystallization a minimum confinement size, which we denote as $|R_{\mathrm{min}}|$, below which the phase transformation is not possible. We now extend these studies by determining the important and necessary connection between this minimum confinement size $|R_{\mathrm{min}}|$ and the size of the critical nucleus. This also enables us to show that below $|R_{\mathrm{min}}|$ the phase transition temperature is determined by the availability of the crystallizing material to produce a thermodynamically feasible transition, rather than the magnitude of the energy barrier.

Vanfleet and Mochel[4] iteratively determined the melting and freezing points expected for homogeneous nucleation as a function of particle radius by using a capillarity approach, combined with a short-range exponential term to account for surface-induced disordering or ordering. Importantly, they found that for sufficiently small particles (i.e., those with radii below $|R_{\mathrm{min}}|$) the energy barrier was so low that it was easily overcome on both melting and freezing and so the hysteresis normally observed between the two disappeared. Our model is similar to theirs and others,[5,6] except that the exponential term is omitted so that we can explicitly derive formulas for onset melting and crystallization temperatures and R_{min}. We also consider the case of heterogeneous nucleation and crystallization from solution, as well as the melt. The absence of an exponential term means that we can account for the presence of a surface premelting or unfreezable layer but not its width. So if such a surface layer exists, then the confinement boundary is located at the junction between this surface layer and the underlying solid/melt, rather than at the junction between the two different materials. This is not detrimental in systems where the width of premelting/unfreezable layers is known.[1] Consequently, the main advances presented in this paper are as follows: first, the establishment of a limiting confinement size below which crystallization is determined by the scarcity of the crystallizing material, rather than the energy barrier to the transition; second, the formulation of the following: (a) readily determinable onset temperatures for melt and solute crystallization via homogeneous and heterogeneous nucleation in confined volumes, (b) the relationship between the nucleation free energy barrier for flat and curved substrates, and (c) the relationship between the size of critical nuclei and sufficiently small confining volumes.

The purpose of this paper is to outline our simple classical model and to detail its uses and limitations. In particular, our mesoscopic model adopts the capillarity approach of

assuming an interface of zero thickness and uses interfacial tensions to describe the interactions between surfaces. The specific molecular interactions between surfaces needed to explain, for example, the occurrence of premelting, are not considered. Many detailed atomistic approaches have already been described to account for this phenomenon in confined geometries.[32–35] The interfacial tension values used in our model for confinement radii above $|R_{\min}|$ are necessarily isotropic, so that the crystallite orientation does not need to be known, and as the confining volume decreases in size, the interfacial tension values should be expected to deviate from the bulk values.[1,36–40] Our model will typically be applied to nuclei of several hundred molecules, though we will also test its applicability in smaller systems, where the concept of an interfacial tension is ill conceived. The aim in this situation is to use the interfacial tension as an adjustable parameter that measures the undersaturation of bonding across an interface, since this descriptor remains valid at the molecular level.[41] The effects of equilibrium fluctuations and phase coexistence in finite systems[42,43] are also neglected, both to retain a simple and readily accessible model, and in the recognition that our model will generally be applied to systems sufficiently large to warrant their exclusion. Despite these limitations, our model is useful because it provides analytical expressions for onset crystallization temperatures in confined volumes that represent an improvement over the often-used CNT, in which all substrate surfaces are assumed to be planar and the crystallization temperature is always determined by the size of the nucleation barrier. Thus our model provides a better framework for comparing classical, capillarity models with experimental and simulation data on crystallization in confined volumes without requiring any additional information. Importantly, our model also reveals how critical nucleus sizes can be obtained simply by measuring the size of sufficiently small confining volumes, as the crystallization is then determined by the thermodynamic feasibility of the transition.

The remainder of this paper is organized as follows. Section II briefly outlines CNT. Section III extends CNT to account for nucleation upon convex and concave substrates and derives onset crystallization temperatures in confined volumes based on this capillarity approach. We then demonstrate in Sec. IV that the onset crystallization temperatures determined from the extended CNT are inappropriate for the smallest confining volumes because the phase transition is determined by the scarcity of the crystallizing material and not the free energy barrier to nucleation. As a result, new formulas for onset crystallization temperatures in the smallest confining volumes are presented, and the connection between these confining volume sizes and the critical nucleus size is established. Finally, in Sec. V we discuss the general applicability of our model and possible improvements, and present concluding remarks in Sec. VI.

II. CLASSICAL NUCLEATION THEORY (CNT)

The formation of any new phase from a bulk parent phase requires the creation of an interface between the two phases, which requires work. Hence there exists an energy barrier to the formation of the new phase, which is given by the Gibbs free energy change ΔG^* for a closed system at constant pressure and temperature and the Helmholtz free energy change ΔF^* for a closed system at constant volume and temperature. Here we are interested in phase transitions in confined volumes, for which ΔF^* is appropriate; however, analogous expressions for ΔG^* are readily obtainable. In CNT,[44] the value of ΔF^*_{hom} for homogeneous nucleation, i.e., nucleation within the bulk parent phase, is calculated as follows. The change in the free energy ΔF_{hom} in forming a spherical crystalline nucleus of n molecules from the melt is given by the sum of favorable volume and unfavorable surface area terms, i.e.,

$$\Delta F_{\text{hom}} = -n\Delta\mu + \Sigma\gamma A_I = -\frac{4\pi r^3\Delta\mu}{3v_c} + 4\pi r^2\gamma, \tag{4}$$

where γ is the interfacial tension between the nucleus and the surrounding melt, A_I is the interfacial area, r is the radius of the nucleus, and v_c is the molecular volume of the crystalline species. The supersaturation $\Delta\mu$ is the driving force for crystallization and is related to the supercooling $\Delta T_c = T_{eq} - T_c$, where T_c is the crystallization temperature, by

$$\Delta\mu = \Delta_{\text{fus}}H\Delta T_c/T_{\text{eq}}, \tag{5}$$

assuming that $\Delta_{\text{fus}}H$ is invariant between T_c and T_{eq}. The barrier to nucleation ΔF^*_{hom} is found from the maximum in ΔF_{hom} by setting $dF_{\text{hom}}/dr=0$. This condition is satisfied when $r=r^*=2\gamma v_c/\Delta\mu$, i.e., by the Gibbs–Thomson equation, and we find that

$$\Delta F^*_{\text{hom}} = \frac{16}{3\Delta\mu^2}\pi\gamma^3 v_c^2. \tag{6}$$

III. EXTENSION OF CNT TO CURVED SUBSTRATES

This approach can be extended to provide the energy barrier for heterogeneous nucleation on convex and concave substrates of radius R, as shown in Fig. 2. In this case, the Helmholtz free energy change ΔF_{het} is given to a first approximation[7] by[24–26]

$$\Delta F_{\text{het}} = -\frac{4}{3v_c}\pi r^3\Delta\mu[f(\theta+\phi) - (R/r)^3 f(\phi)] + 2[1-\cos(\theta+\phi)]\pi r^2\gamma + 2(1-\cos\phi)\pi R^2(\gamma_2-\gamma_1), \tag{7}$$

where θ is the contact angle between the nucleus and the spherical substrate, ϕ is the angle between the spherical substrate and the plane connecting the nucleus edge, $f(\alpha) = 0.25(2-3\cos\alpha+\cos^3\alpha)$, and γ_1 and γ_2 are the interfacial tensions between the substrate and bulk phase, and substrate and nucleus, respectively, see Fig. 2. Note that for the concave surface system, corresponding to crystallization within the curved substrate, R and ϕ are assigned negative values. In Eq. (7) the supersaturation is invariant with R, as the molecular volumes of the daughter and parent phases are assumed equal. The removal of this assumption would lead to an additional term $(v_0-v_c)\Delta P$ in Eq. (7), where v_0 is the

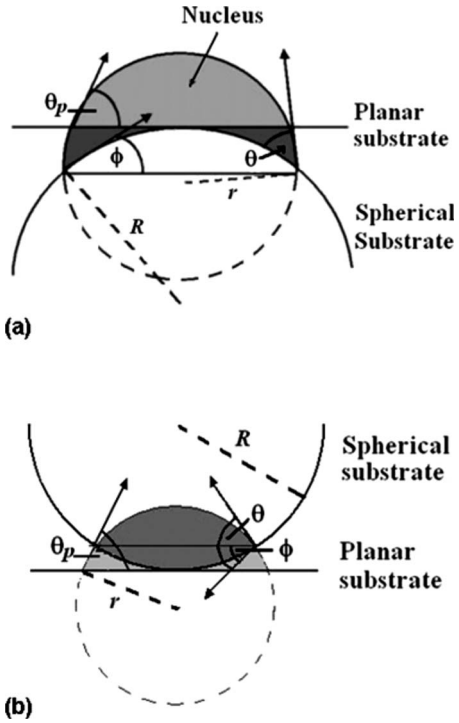

FIG. 2. Schematic diagram describing nucleation upon (a) convex and (b) concave substrates of radius, R. In (a) the combined light and dark gray regions depict the nucleus on the convex substrate, whereas in (b) the dark gray regions depict the nucleus on the concave surface.

molecular volume of the crystallizing species in its parent phase and ΔP is the pressure difference across the curved surface. This term arises due to the effect of pressure on the chemical potentials of the parent and daughter phases.[27] For crystallization within microemulsion droplets, which we are most interested in, the value of ΔP is sufficiently small that this term can be assumed to have little effect on the supersaturation even when the assumption $v_0=v_c$ is not valid.[45,46] Indeed, the low value of ΔP is a necessary requirement for microemulsions, as otherwise these phases would not be thermodynamically stable.

From Young's equation, $\cos\theta=(\gamma_1-\gamma_2)/\gamma$, so Eq. (7) becomes

$$\Delta F_{\text{het}} = -\frac{4}{3v_c}\pi r^3\Delta\mu[f(\theta+\phi)-(R/r)^3 f(\phi)] + 2[1-\cos(\theta+\phi)]\pi r^2\gamma - 2\cos\theta(1-\cos\phi)\pi R^2\gamma. \quad (8)$$

The maximum in ΔF_{het} gives the barrier to nucleation ΔF^*_{het}, and again this condition is satisfied[24,26] when $r=r^*=2\gamma v_c/\Delta\mu$.

Hence

$$\Delta F^*_{\text{het}} = \frac{32}{3\Delta\mu^2}\pi\gamma^3 v_c^2[-f(\theta+\phi)+(R/r^*)^3 f(\phi)] + \frac{8}{\Delta\mu^2}\pi\gamma^3 v_c^2[\{1-\cos(\theta+\phi)\}-\cos\theta(1-\cos\phi)\times(R/r^*)^2].$$

Rearrangement and simplification give

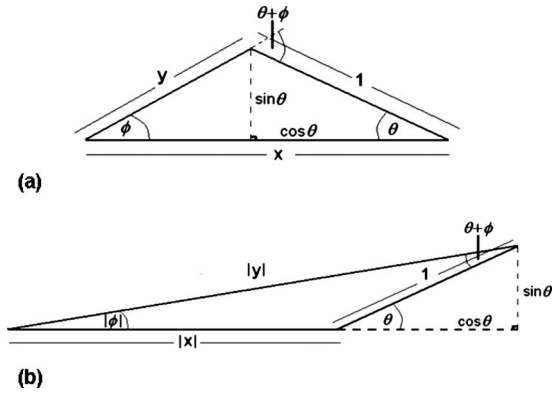

FIG. 3. Diagram showing the geometric relationships between x, y, θ, ϕ, and $(\theta+\phi)$ for (a) the convex surface system and (b) the concave surface system.

$$\Delta F^*_{\text{het}} = \frac{\Delta F^*_{\text{hom}}}{2}[1-\cos^3(\theta+\phi)+4x^3 f(\phi) - 3x^2\cos\theta(1-\cos\phi)], \quad (9)$$

where $x=R/r^*$. This equation applies to nucleation upon both the outer and inner surfaces of a spherical substrate, to give the convex and concave (R, $\phi<0$) surface cases shown in Figs. 2(a) and 2(b), respectively.

Greater insight into Eq. (9) is provided by introducing the variable y, where

$$y = \pm(x^2-2x\cos\theta+1)^{0.5}. \quad (10)$$

The positive and negative roots apply to a nucleus on convex and concave surfaces, respectively. The variable $|y|$ represents the third side of a triangle whose other two lengths are 1 and $|x|$, with the angle between the sides of 1 and $|x|$ being θ for the convex surface case and $(180°-\theta)$ for the concave surface case. The angle between the sides of lengths $|y|$ and $|x|$ is then $|\phi|$, see Fig. 3.

Using this we find that $\cos\phi=(x-\cos\theta)/y$ and $\cos(\theta+\phi)=(x\cos\theta-1)/y$. After substitution and simplification, Eq. (9) then becomes

$$\Delta F^*_{\text{het}} = \frac{\Delta F^*_{\text{hom}}}{2}\{1-3x^2\cos\theta+2x^3 + y(1+x\cos\theta-2x^2)\} = \Delta F^*_{\text{hom}} f(\theta_p), \quad (11)$$

where θ_p is the angle between the corresponding planar critical nucleus and the plane tangential to the curved substrate surface, as shown in Fig. 2. Hence the heterogeneous nucleation barrier for any size concave or convex substrate can be predicted by determining the value of θ_p. θ_p is given simply by

$$\cos\theta_p = x-y. \quad (12)$$

A proof of the equivalence of the right hand side (RHS) of Eqs. (9) and (11) is given in Appendix A. Equation (11) shows that at a given temperature, and hence constant ΔF^*_{hom} value, ΔF^*_{het} depends only on the θ_p value. Consequently, in Fig. 4, all the spherical substrates depicted result in the same ΔF^*_{het} value. This can be rationalized as follows. For nucleation on a concave surface, the critical nucleus volume v^* is

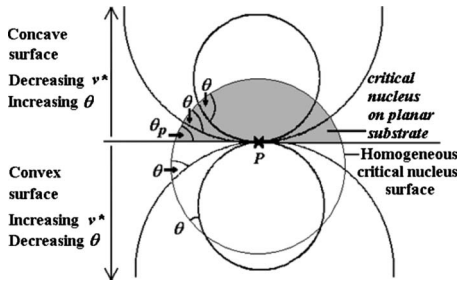

FIG. 4. Schematic diagram showing that for a given supersaturation and hence critical nucleus radius r^*, all surfaces through point P that cross the homogeneous critical nucleus surface (Ref. 47) produce the same ΔF^*_{het} value for nucleation, since they all have the same θ_p value.

reduced compared to the planar case, and hence fewer molecules need to cluster together to form the critical nucleus. However, this effect is negated by the greater contact angle θ compared to θ_p, which means that more work is required to create unit area of the nucleus-substrate interface and so the mean energy increase on the addition of a molecule to the subcritical nucleus is larger. In contrast, for nucleation on a convex substrate, v^* is increased compared to the planar case, but θ is decreased, see Fig. 5.

We have obtained the energy barrier to nucleation ΔF^*_{het} and now wish to find the onset temperature for the phase transition, i.e., the highest temperature T_{trans} at which the transition should be observable. This is achieved by setting the nucleation rate J_{trans} at T_{trans} to a suitable detection limit, where $J_{\text{trans}}=A\exp(-\Delta F^*_{\text{het}}/kT_{\text{trans}})$ and A is the pre-exponential factor, which can be considered constant over a relatively narrow temperature range.[51] Using $(\Delta F^*_{\text{het}}/k)=(T_{\text{eq}}-\Delta T_{\text{trans}})\ln(A/J_{\text{trans}})$, where $\Delta T_{\text{trans}}=T_{\text{eq}}-T_{\text{trans}}$, and substituting in Eqs. (11), (6), and (5) in turn, this gives

$$\Delta T^3_{\text{trans}}-\Delta T^2_{\text{trans}}T_{\text{eq}}+\frac{16\pi\gamma^3 v_c^2 T_{\text{eq}}^2 f(\theta_p)}{3k\Delta_{\text{fus}}H^2\ln(A/J_{\text{trans}})}=0. \tag{13a}$$

Equation (13a) can be rewritten to show the connection between R and ΔT_{trans} by substituting for $f(\theta_p)$, see Eq. (11), to give

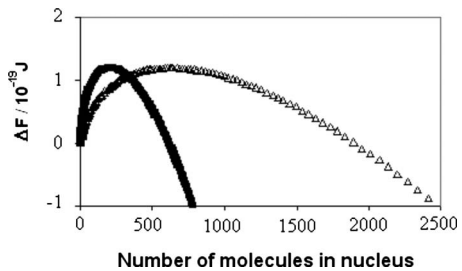

FIG. 5. Graph of ΔF_{het} vs number of molecules in an ice nucleus at $T_c=251$ K for concave (filled squares) and convex (unfilled triangles) substrates of the same radius, 2.1 nm, with the same r^* value of 2.1 nm and the same θ_p value of 73.4° when $r=r^*$. This corresponds to systems with a contact angle of 100° for the concave surface case and 41.9° for the convex one. Values (Refs. 48–50) of $v_c=3.26\times10^{-29}$ m^3, $\gamma=22$ mN m^{-1}, and $\Delta_{\text{fus}}H=5000$ J mol^{-1} have also been used in Eq. (8).

$$\begin{aligned}&\Delta T^3_{\text{trans}}-\Delta T^2_{\text{trans}}T_{eq}\\&\quad+C(1-3D^2R^2\Delta T^2_{\text{trans}}\cos\theta+2D^3R^3\Delta T^3_{\text{trans}})\\&=C(D^2R^2\Delta T^2_{\text{trans}}-2DR\Delta T_{\text{trans}}\cos\theta+1)^{0.5}\\&\quad\times(1+DR\Delta T_{\text{trans}}\cos\theta-2D^2R^2\Delta T^2_{\text{trans}}),\end{aligned} \tag{13b}$$

where $C=8\pi\gamma^3v_c^2T_{\text{eq}}^2/3k\Delta_{\text{fus}}H^2\ln(A/J_{\text{trans}})$ and $D=x/R\Delta T_{\text{trans}}=1/r^*\Delta T_{\text{trans}}=\Delta_{\text{fus}}H/2\gamma v_cT_{\text{eq}}$.

On squaring Eq. (13b), canceling like terms on the left hand side and RHS and dividing through by $\Delta T^2_{\text{trans}}$ (providing the nonphysical root $\Delta T_{\text{trans}}=0$), a quartic equation in ΔT_{trans} emerges, namely,

$$\begin{aligned}&\Delta T^4_{\text{trans}}(1+4CD^3R^3)-2\Delta T^3_{\text{trans}}(T_{\text{eq}}+3CD^2R^2\cos\theta\\&\quad+2CD^3R^3T_{\text{eq}})+\Delta T^2_{\text{trans}}(T^2_{\text{eq}}+6CD^2R^2T_{\text{eq}}\cos\theta)\\&\quad+2\Delta T_{\text{trans}}(C+2C^2D^3R^3-3C^2D^3R^3\cos\theta\\&\quad+C^2D^3R^3\cos^3\theta)-2CT_{\text{eq}}-6C^2D^2R^2\cos\theta\\&\quad+3C^2D^2R^2(1+\cos^2\theta)=0.\end{aligned} \tag{13c}$$

Equation (13c) can be solved analytically with R, θ, T_{eq}, v_c, γ, $\Delta_{\text{fus}}H$, and A/J_{trans} as inputs. Four real roots arise, one of which provides the expected onset phase transition temperature. The remaining three roots are all unphysical and can be discarded. Two of these unphysical roots derive from the squaring procedure used to obtain Eq. (13c), which means that the stipulation that y values must be negative for concave curvature systems can no longer be enforced. The remaining unphysical root gives an onset crystallization temperature approaching 0 K, where the critical nucleus contains only one molecule and the energy barrier is vanishingly small. Crystallization would not be observed at this temperature, of course, as freezing at the higher T_c (or vitrification in the case of a sufficiently rapid quench) would have already occurred prior to this.

A simpler analytical solution to Eq. (13a) can also be found as follows. Crucially, in Eq. (13a), $f(\theta_p)$ can be obtained with x and θ as inputs, as x and θ are independent variables. Once the value of $f(\theta_p)$ is known from specifying x and θ, Eq. (13a) becomes cubic, and it can be solved analytically. The onset crystallization temperature T_c, where $T_c\leq T_{\text{eq}}$ is then given by

$$T_c=\frac{T_{\text{eq}}}{3}\{2+\cos W-(3^{0.5}\sin W)\}, \tag{14}$$

where

$$W=\frac{1}{3}\arccos\left[1-\frac{72\pi\gamma^3v_c^2f(\theta_p)}{k\Delta_{\text{fus}}H^2T_{\text{eq}}\ln(A/J_{\text{trans}})}\right].$$

Hence T_c can be found with x, θ, T_{eq}, v_c, γ, $\Delta_{\text{fus}}H$, and A/J_{trans} as inputs. r^* and R can then be obtained from the Gibbs–Thomson equation and $R=r^*x$, respectively. The second solution to Eq. (13a) provides the expected onset melting temperature T_m for a nucleation-based melting transition, which would be required in the absence of a surface liquid layer. T_m is given by

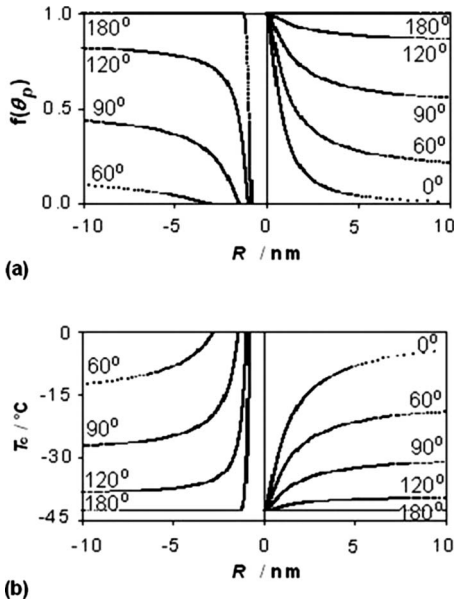

FIG. 6. The predicted variation in (a) $f(\theta_p)$ and (b) the ice onset crystallization temperatures, respectively, as a function of R for different contact angle systems. Negative and positive R values relate to crystallization on concave and convex substrates, respectively.

$$T_m = \frac{T_{eq}}{3}\{2 + \cos W + (3^{0.5} \sin W)\}. \quad (15)$$

Note that T_c and T_m can both be found from the cubic form of Eq. (13a) as the transition enthalpy appears only through its square. The third solution, $T_c=(2T_{eq}/3)\{1-\cos W\}$ represents the nonphysical case where T_c is approaching 0 K and so the critical nucleus contains only one molecule and the energy barrier is vanishingly small. Equations (14) and (15) are valid for nucleation on any shaped substrate, provided the appropriate geometric factor g is included in determining W, i.e.,

$$W = \frac{1}{3}\arccos\left[1 - \frac{72\pi\gamma^3 v_c^2 g}{k\Delta_{fus}H^2 T_{eq}\ln(A/J_{trans})}\right],$$

and for a spherical substrate, $g=f(\theta_p)$, whereas for a planar substrate $g=f(\theta)$.

Figures 6(a) and 6(b) show the predicted variation in $f(\theta_p)$ and the ice onset crystallization temperatures T_c, respectively, as a function of substrate radius R, for different contact angle systems. The ice onset crystallization temperatures have been determined using reasonable values[48–50] of $v_c=3.26\times10^{-29}$ m^3, $\gamma=22$ mN m^{-1}, $\Delta_{fus}H=5000$ J mol^{-1} and $A/J_{trans}=10^{15}$ for the heterogeneous nucleation case, and values of $v_c=3.26\times10^{-29}$ m^3, $\gamma=20$ mN m^{-1}, $\Delta_{fus}H=4060$ J, and $A/J_{trans}=10^{18}$ for homogeneous nucleation. For the convex surface case, x and y are positive, $y \geq x-\cos\theta$, and $\theta_p \geq \theta$, see Eqs. (10) and (12). For the concave surface case, x and y are negative, $|y| \geq |x|+\cos\theta$, and so $\theta_p \leq \theta$. Consequently, nucleation is easier on a concave surface compared to a convex one with the same θ value, and the difference becomes greater, the smaller the magnitude of x. Indeed, for the concave surface case, as $|x|$ approaches zero, θ_p tends to 0° owing to the reduction in the critical nucleus size. In contrast, as $|x|$ tends to zero for the convex surface case, θ_p tends to 180°, and the critical nucleus size and onset crystallization temperature tend to the corresponding homogeneous nucleation values.

Equation (13a) can also be applied, within the limitations of the classical theory, to the cases of homogeneous nucleation and the melting of small particles with a surface liquid layer, see Appendix B. From this, it would appear that the phase transition temperature T_{trans} for any system in a confined volume can be predicted by determining the value of $f(\theta_p)$ from the correctly signed values of x and y and then using either Eq. (14) or Eq. (15), as appropriate, see Table I.[52]

We now show, however, that for the smallest confining volumes, Eq. (13a) is inappropriate because the phase transition temperature is no longer determined by the magnitude of the energy barrier to the transition.

IV. PHASE TRANSITIONS WITHIN SMALL CONFINED VOLUMES

A. Crystallization from the melt and melting

Consider the heterogeneous nucleation of a confined phase with a crystallization contact angle of $\theta_c=\arccos[(\gamma_1-\gamma_2)/\gamma]$. In the absence of surface melting, we would expect melting of this *same* system to occur by a heterogeneous nucleation mechanism for which the melting contact angle $\theta_m \sim \arccos[(\gamma_2-\gamma_1)/\gamma]$, i.e., $\sim 180°-\theta_c$. θ_m will be exactly $180°-\theta_c$ if the nucleus structure is equivalent to that of the new phase produced within the substrate, and so this will be more likely as R approaches r^*. Figures 7(a) and 7(b) show the predicted ice onset crystallization and melting temperatures in the absence of surface melting obtained from Eqs. (14) and (15) for the case of (a) $\theta_c=80°$,

TABLE I. Parameter signs and equation numbers for predicting onset crystallization and melting temperatures on concave and convex surfaces.

System	Process	Relative T_{trans} value	R	y	r^*	x	Physical θ_p?[a]	Equation No. for T_{trans}
Concave	Cryst.	$T_c \leq T_{eq}$	−ve	−ve	+ve	−ve	√	(14)
	Melt	$T_m \geq T_{eq}$	−ve	−ve	+ve	−ve	√	(15)
	Cryst	$T_c \geq T_{eq}$	−ve	−ve	−ve	+ve	X	(15)
	Melt	$T_m \leq T_{eq}$	−ve	−ve	−ve	+ve	X	(14)
Convex	Cryst.	$T_c \leq T_{eq}$	+ve	+ve	+ve	+ve	√	(14)
	Melt	$T_m \geq T_{eq}$	+ve	+ve	+ve	+ve	√	(15)

[a]Reference 52.

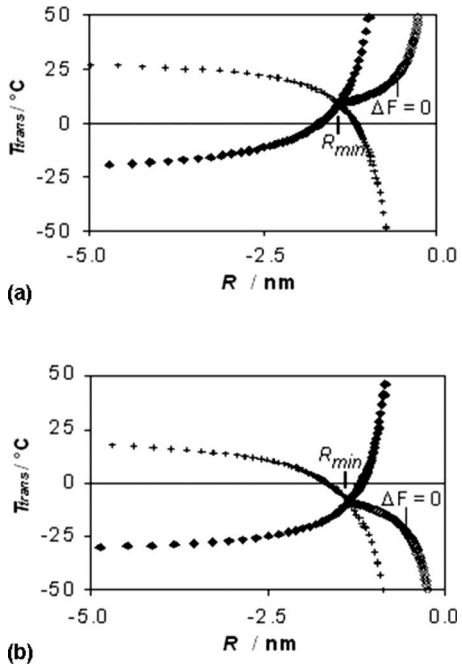

FIG. 7. The predicted ice onset crystallization (filled diamonds) and melting temperatures (crosses) in the absence of surface melting as a function of substrate radius R for heterogeneous crystallization within the substrate. (a) $\theta_c=80°$, $\theta_m=100°$ and (b) $\theta_c=100°$, $\theta_m=80°$. Note that for $|R|<|R_{\min}|$, the ice onset melting and crystallization temperatures are both given by the curve labeled $\Delta F=0$, as the transformation temperature is now determined by the condition that the nucleus grows to a size, r_0.

$\theta_m=100°$ and (b) $\theta_c=100°$, $\theta_m=80°$. The crystallization and melting curves cross at $T_c>T_{\text{eq}}$ if $\theta_c<90°$ and at $T_c<T_{\text{eq}}$ if $\theta_c>90°$. We denote the substrate radius at which the crossing occurs as $R_{\min}$. For all substrate radii smaller than $|R_{\min}|$, we then have the unphysical situation that the melting curve is below the crystallization one, since a fundamental thermodynamic criterion is being violated. In particular, the crystallization and melting curves for $|R|<|R_{\min}|$ correspond to systems where the complete phase transformation results in an increase in the free energy of the system, which of course cannot occur globally across the sample. This arises because, although the critical nucleus size can be attained as ΔF^*_{het} is surmountable, there is then insufficient material within the confining substrate for the free energy change to decrease to zero on further nucleus growth, e.g., in Fig. 1, the nucleus cannot grow to a size r_0. In fact, the limiting criterion that the free energy change must not be greater than zero has long been associated[9] with the minimum possible melting temperature of a small particle. Here we are just extending this idea by also identifying the same criterion with the maximum possible freezing temperature of a confined object.[4,53]

The value of $R_{\min}$ is easily found from the condition that $\Delta F=0$ on complete crystallization. It is given by

$$R_{\min}=\frac{3v_c(\gamma_1-\gamma_2)}{\Delta\mu}=\frac{3v_c\gamma}{\Delta\mu}\cos\,\theta_c=\frac{3r^*}{2}\cos\,\theta_c, \tag{16}$$

where we have retained the convention that substrate radii R must take negative values for nucleation on a concave surface. Equation (16) shows that the $R_{\min}$ condition occurs at $T_c<T_{\text{eq}}$ for $\theta_c>90°$ as $r^*>0$, and at $T_c>T_{\text{eq}}$ for $\theta_c<90°$ since $r^*<0$, see Appendix B. For substrate sizes below $|R_{\min}|$, T_c and T_m are no longer given by Eqs. (14) and (15) but by Eqs. (16) and (5) to give

$$T_c=T_m=T_{\text{eq}}\left[1+\frac{3\gamma v_c\cos\,\theta_c}{|R|\Delta_{\text{fus}}H}\right]. \tag{17}$$

So in Fig. 7, the onset crystallization and melting temperature curves necessarily cross at $R_{\min}$, since at this point they both describe the $\Delta F=0$ condition in going from/to a completely liquid droplet to/from a completely crystalline one. For $|R|\le|R_{\min}|$, the ice onset crystallization and melting temperatures are both given by the curve labeled $\Delta F=0$. Hence, we would expect the hysteresis normally observed upon heating and cooling the *same* system to disappear for phase transformations confined to within volumes with $|R|\le|R_{\min}|$. As required, Eq. (17) reduces to the lower bound of the melting temperature, Eq. (2), when $\theta_m=0$, $\theta_c=180°$ and a surface premelting layer is present. A similar dependence of $\Delta T_{\text{trans}}\propto 1/R$ would also be expected to apply for the limiting criterion that $\Delta F_{\text{het}}=0$ on complete phase transformation within any closed system, but again use of a geometric factor would be required for the correct dependence, e.g., for a cylindrical vessel, $\Delta T_c=(-2\gamma v_c T_{eq}\cos\,\theta_c)/|R|\Delta_{\text{fus}}H$.[6]

When $|R|\le|R_{\min}|$, Eq. (16) holds, i.e., $r^*=2R/(3\cos\,\theta)$, and the critical nucleus size can be obtained if R and θ are known. This is an important finding because determination of r^* usually relies on the Gibbs–Thomson equation and the inappropriate application of bulk interfacial tension values to small nuclei. The number of molecules n^* in the critical nucleus is then given by

$$n^*=\frac{v^*}{v_c}=\frac{4\pi|R|^3}{3v_c}\left\{\frac{1}{2}-\frac{4}{27\cos^3\,\theta}\times\left(1-\frac{2-(3/4)\cos^2\,\theta+(9/8)\cos^4\,\theta}{(4-3\cos^2\,\theta)^{0.5}}\right)\right\}. \tag{18}$$

Crucially we find that the dependence of n^* on θ is relatively weak, so that even if the contact angle can only be estimated to within ~10%, the number of molecules in the critical nucleus is known with good precision if R can be measured. Hence, reliable values of n^* can be found for single crystallization experiments in confined volumes with $|R|\le|R_{\min}|$, where the simple nucleation theorem connection $n^*=(\partial(kT\ln J)/\partial\Delta\mu)_{V,T}$ is not valid. If homogeneous nucleation is occurring ($\theta=180°$), Eqs. (16) and (18) simplify to $r^*=-2R/3$ and $n^*=32\pi|R|^3/81v_c$, so experimental measurement of R directly gives r^* and n^*. This allows a simple and direct measurement of the critical nucleus size for the first time, as we have shown recently for ice crystallization in AOT microemulsions.[1]

An estimate of n^* is also possible based only on the relative value of T_c compared to T_{eq}. In particular, $v^*<0.5V$, where V is the confinement volume, for a heterogeneous nucleation with $T_c<T_{\text{eq}}$ (i.e., $\theta_c>90°$), otherwise the interfacial area, and hence dF/dr, would be decreasing on formation of the critical nucleus. In contrast, for a heterogeneous nucleation with $T_c>T_{\text{eq}}$ (i.e., $\theta_c<90°$), $v^*>0.5V$. For homogeneous nucleation, $v^*=8V/27$.

By using Eq. (13a) for confining substrates with $|R| \geq |R_{\min}|$ and Eq. (17) for substrates with $|R| \leq |R_{\min}|$, the entire T_c and T_m versus R dependence can be modeled. These equations can be used to model the onset melting and crystallization temperature variation with confinement volume for any system, within the limitations of our model, i.e., the assumption of an infinitely thin interface, incompressible phases, no volume change on phase transformation, and the isotropic nature of the critical nucleus and confining volume. For a constant $\theta_c > 90°$, we expect a drop-off in onset crystallization temperatures for sufficiently small confinement volumes, which is seen in many systems.[2,3] The drop-off rate will be mediated, though, by any change in the contact angle and deviation of the ratio $\gamma/\Delta_{\text{fus}}H$ from its bulk value. In contrast, for a constant $\theta_c < 90°$, we expect the far rarer case of an increase in onset crystallization temperatures for sufficiently small confinement volumes, as has been observed for CCl_4 freezing in microporous activated carbon fibers.[54]

Please note that Eq. (17) assumes that γ, θ, and $\Delta_{\text{fus}}H$ are invariant with R, but for very small confinement sizes, γ and $\Delta_{\text{fus}}H$ are expected to deviate from their bulk values. The value of θ is also likely to increase as $|R|$ decreases, as we have previously observed.[25] However, the variation of γ, θ, and $\Delta_{\text{fus}}H$ from their bulk values can be ascertained by measuring the extent to which the gradient of a $\ln|R|$ versus $\ln \Delta T_c$ plot deviates from -1. Also for homogeneous nucleation, and other cases where the contact angle value is known, we can evaluate how the ratio $\gamma/\Delta_{\text{fus}}H$ differs from its bulk value. For instance, the water-ice interfacial tension value was found to be significantly reduced from its bulk value for ice crystallization in microemulsion droplets of sub-2 nm water pool radius.[1] This provides an independent measure of how highly curved nanoscale systems perturb the bulk ratio values of $\gamma/\Delta_{\text{fus}}H$.

B. Crystallization of solutes in confined volumes

Our model can be extended to crystallization of solutes, though here the situation is complicated by the decrease in supersaturation that arises as the nucleus grows. Reguera *et al.* previously derived[8] an EMDL model for homogeneous nucleation from the vapor in confined volumes accounting for the depletion of vapor molecules as the nucleus grows. Our solute crystallization treatment is analogous to theirs except that we consider the heterogeneous nucleation case as well, but we do not include the effects of fluctuations and the very small volume work term, which is commonly ignored. The free energy change on solute crystallization for an ideal solution is then given by

$$\Delta F = -nkT \ln\frac{c_1}{c_{eq}} + \Sigma \gamma A_I + NkT\left\{\ln\left(1-\frac{v}{Vv_c c_0}\right) - \frac{1}{v_c c_0}\ln\left(1-\frac{v}{V}\right)\right\}, \quad (19)$$

where n is the number of molecules in the nucleus, c_1 is the solute concentration for that particular nucleus size, with $c_1 = c_0(1-v/Vv_c c_0)(1/1-v/V)$, c_0 is the initial solute concentration when $n=0$, v is the nucleus volume, V is the spherical confining volume, v_c is the molecular volume of the crystalline species, c_{eq} is the equilibrium solute concentration at that temperature T, so for an ideal solution this is given by $c_{\text{eq}} = \exp[(-\Delta_{\text{fus}}H/kT) + \text{const}]$, and N is the initial number of solute molecules when $n=0$.

The free energy difference ΔF now exhibits a maximum ΔF_a^* corresponding to the critical nucleus radius r_a^* and a minimum ΔF_b^* at a larger nucleus radius r_b^*, owing to the decrease in the supersaturation as the nucleus grows. r_a^* and r_b^* are both given by the usual Gibbs–Thomson equation with both ΔF_a^* and ΔF_b^* given by

$$\Delta F^* = \frac{16\pi\gamma^3 v_c^2 T_{\text{eq}}^2 f(\theta_p)}{3\Delta_{\text{fus}}H^2 \Delta T_c^2} + NkT\left\{\ln\left(1-\frac{v^*}{Vv_c c_0}\right) - \frac{1}{v_c c_0}\ln\left(1-\frac{v^*}{V}\right)\right\}, \quad (20)$$

where v^* is the nucleus volume when $r=r^*$, with the subscripts a and b then used to distinguish the maximum and minimum values, respectively, and T_{eq} is the saturation temperature for the solution at concentration c_{1a}^* surrounding the critical nucleus r_a^*. The ratio v^*/V depends only on x and θ and is given by

$$\frac{v^*}{V} = \frac{f(\theta+\phi)}{x^3} - f(\phi) = \frac{1}{|x^3|}\left\{\frac{1}{2} - \frac{x^3}{2} + \frac{2-2x\cos\theta + x^2 - x^2\cos^2\theta - 2x^3\cos\theta + 2x^4}{4y}\right\}.$$

As before, the onset crystallization temperature is found from $(\Delta F_a^*/kT_c) = \ln(A/J_{\text{trans}})$, with A assumed constant. Using $N = (-32\pi c_0/3)(\gamma v_c T_{eq} x_a/\Delta_{\text{fus}}H)^3(1/\Delta T_c^3)$, the equation

$$\Delta T_c^4 - T_{\text{eq}}\Delta T_c^3 + (X-Y)\Delta T_c + T_{\text{eq}}Y = 0 \quad (21)$$

is obtained, where $X = 16\pi\gamma^3 v_c^2 f(\theta_{p,a}) T_{eq}^2/3k\ln(A/J_{\text{trans}})\Delta_{\text{fus}}H^2$ and $Y = -(32\pi c_0/3\ln(A/J_{\text{trans}})) \times (\gamma v_c T_{eq} x_a/\Delta_{\text{fus}}H)^3\{\ln(1-v^*/Vv_c c_0) - (1/v_c c_0)\ln(1-v^*/V)\}$. Equation (21) reduces to Eq. (13a) when $Y=0$. Note that it is not possible now to provide a purely power law expression relating R and ΔT_c, as was done for the melt crystallization case, see Eq. (13c), owing to the $\ln(1-v^*/V)$ and $\ln(1-v^*/Vv_c c_0)$ terms present in Eq. (21). Instead, solutions to Eq. (21) must be found numerically if R, θ, c_0, T_{eq}, v_c, γ, $\Delta_{\text{fus}}H$, and A/J_{trans} are used as inputs, with each R value providing one physically meaningful solution, i.e., the required onset crystallization temperature. Alternatively, an analytical solution to Eq. (21) is possible as follows. We can find $f(\theta_{p,a})$ and v_a^*/V by first specifying the independent variables, x_a and θ. c_{1a}^* and hence T_{eq} are then obtained from v_a^*/V and the third independent variable c_0. Once $f(\theta_{p,a})$, v_a^*/V, and T_{eq} are known, Eq. (21) becomes quartic and therefore it is solvable with x_a, θ, c_0, T_{eq}, v_c, γ, $\Delta_{\text{fus}}H$, and A/J_{trans} as inputs. For the typical case where $T_c \leq T_{\text{eq}}$, T_c is then given by

$$T_c = \frac{3T_{\text{eq}}}{4} + z_1^{0.5} + z_2^{0.5} - z_3^{0.5}, \quad (22)$$

where

$$z_1 = \left\{ -\left[\frac{T_{eq}(X+3Y)}{48} \right]^{0.5} \times \left(\cos\left(\frac{Z}{3}\right) - 3^{0.5} \sin\left(\frac{Z}{3}\right) \right) \right\} + \frac{T_{eq}^2}{16},$$

$$z_2 = \left\{ -\left[\frac{T_{eq}(X+3Y)}{48} \right]^{0.5} \times \left(\cos\left(\frac{Z}{3}\right) + 3^{0.5} \sin\left(\frac{Z}{3}\right) \right) \right\} + \frac{T_{eq}^2}{16},$$

and

$$z_3 = \left\{ \left[\frac{T_{eq}(X+3Y)}{12} \right]^{0.5} \cos\left(\frac{Z}{3}\right) \right\} + \frac{T_{eq}^2}{16},$$

where $Z=\arccos\{27^{0.5}[T_{eq}^3 Y+(X-Y)^2]/2[T_{eq}(X+3Y)]^{1.5}\}$. r_a^* and R are then found from the Gibbs–Thomson equation and $R=r_a^* x_a$, respectively.

Of the other three solutions to the quartic Eq. (21), two are nonphysical, as they correspond to either crystallization close to 0 K or the onset crystallization temperature close to T_{eq} found when the minimum free energy radius r_b^* is used instead of the maximum value r_a^*. The third solution provides the onset crystallization temperature for rare cases when $T_c > T_{eq}$, which could in principle arise for sufficiently soluble species when $\theta < 90°$. In this case, positive values of x are used since r is negative as well as R (see the analogous melt crystallization case in Table I) and $T_c = 3T_{eq}/4 + z_1^{0.5} - z_2^{0.5} + z_3^{0.5}$.

As with the melt crystallization case, Eqs. (21) and (22) are valid until the confinement size decreases to such an extent that there is insufficient crystallizing material present to ensure an energetically feasible phase transformation. For these small confinement volumes, where $|R| \le |R_{min}|$, we set the *minimum* energy ΔF_b^* when $r=r_b^*$ to zero, to obtain

$$R = \frac{\gamma f(\theta_{p,b})}{kT_c c_0 x_b^2 \left\{ \ln\left(1 - \frac{v_b^*}{V v_c c_0}\right) - \frac{1}{v_c c_0} \ln\left(1 - \frac{v_b^*}{V}\right) \right\}} = \frac{2\gamma v_c x_b}{kT_c \ln(c_{1b}^*/c_{eq})}, \quad (23)$$

from which we get

$$x_b = \frac{R}{r_b^*} = \left(\frac{\ln(c_{1b}^*/c_{eq}) f(\theta_{p,b})}{2 v_c c_0 \ln\left(1 - \frac{v_b^*}{V v_c c_0}\right) - 2 \ln\left(1 - \frac{v_b^*}{V}\right)} \right)^{1/3},$$

or

$$x_b = \frac{R}{r_b^*} = f(\theta_{p,b})^{1/3} \times \left(\frac{\ln c_0 - \ln c_{eq} + \ln\left(1 - \frac{v_b^*}{V v_c c_0}\right) - \ln\left(1 - \frac{v_b^*}{V}\right)}{2 v_c c_0 \ln\left(1 - \frac{v_b^*}{V v_c c_0}\right) - 2 \ln\left(1 - \frac{v_b^*}{V}\right)} \right)^{1/3}, \quad (24)$$

where v_b^* is the volume of the r_b^* nucleus with $\Delta F=0$, $\partial \Delta F/\partial r=0$, and $\partial^2 \Delta F/\partial r^2 > 0$, and c_{1b}^* is the solute concentration surrounding the r_b^* nucleus. Equation (24) can be solved iteratively to give x_b with inputted values for c_0, θ, v_c, and c_{eq} (determined from solubility data and T_c) but again crucially not the γ or $\Delta_{fus}H$ values. The x_a value is then given by

$$\frac{x_a}{\ln(c_{1a}^*/c_{eq})} = \frac{x_b}{\ln(c_{1b}^*/c_{eq})}. \quad (25)$$

Thus we can work out $r_a^* = R/x_a$ just by measuring R and T_c values, when $|R| \le |R_{min}|$. The number of molecules n^* $(=v_a^*/v_c)$ in the critical nucleus is also obtained from just R, θ, c_0, v_c, and T_c as inputs and is given by

$$n^* = \frac{4\pi R^3}{3 v_c x_a^3} \left\{ \frac{1}{2} - \frac{x_a^3}{2} + \frac{2 - 2x_a \cos\theta + x_a^2 - x_a^2 \cos^2\theta - 2x_a^3 \cos\theta + 2x_a^4}{4y} \right\}. \quad (26)$$

Hence for $|R| \le |R_{min}|$, and a known or estimated θ, we can determine both n^* and r_a^* without reliance on macroscopic γ and $\Delta_{fus}H$ values. The experimental onset crystallization temperature can then be compared with the values predicted from the Gibbs–Thomson and ideal solubility equations using the experimentally found R, x, and c_{eq} values. This allows the validity of these equations to be deduced and provides a measure of how bulk values of γ and $\Delta_{fus}H$ are likely to be perturbed for solute crystallization in nanosystems. Please note, though, that when comparing experimental and predicted onset crystallization temperatures for crystallization from solution, the assumption of an infinitely thin interface may result in substantial discrepancies if the solute material is also absorbed within the interfacial region. However, this possibility can be accounted for by determining the solubility of the solute material in the microemulsions in the temperature range of interest, as shown by Yano *et al.*[55]

Figure 8 shows the variation in T_c with R predicted for octadecane in dodecane solutions with different θ values assuming that the crystallization occurs via nucleation of a metastable rotator phase[56–59] with values[56] of $\gamma = 6.2$ mN m^{-1}, $\Delta_{fus}H = 42.012$ kJ mol^{-1}, $v_c = 5.44 \times 10^{-28}$ m^3, $A/J_{trans} = 10^{15}$, and $T_m = 300.15$ K. This system was chosen as it would be expected to show close to ideal solution behavior, though of course the critical nucleus may deviate from cap shaped. For $\theta > 90°$, the curves show an approximately constant T_c until ~2–10 nm, after which T_c falls sharply [see Figs. 8(a) and 8(b)]. For $\theta < 90°$, however,

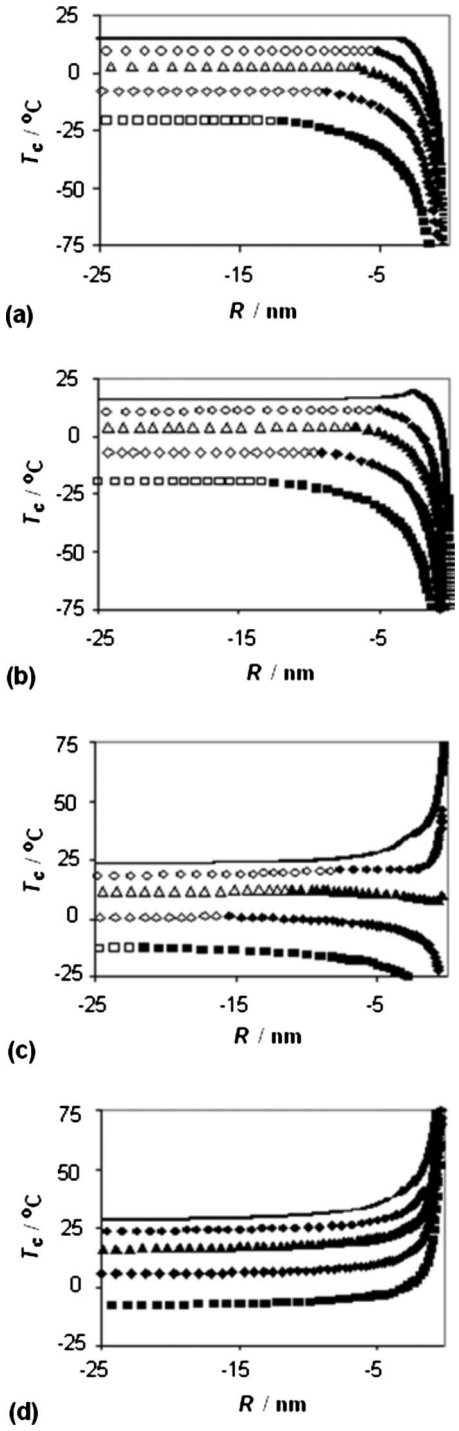

FIG. 8. Graphs showing the variation in onset crystallization temperature T_c with confinement radius R for solutions of octadecane in dodecane for varying mole fractions and the following contact angles: (a) 180° (homogeneous case), (b) 120°, (c) 60°, and (d) 1°. The open symbols correspond to the regime where $\Delta F_a^*=kT_c \ln(A/J_{\text{trans}})$ gives T_c, the filled symbols to the regime where $|R|\leq|R_{\text{min}}|$ and T_c is controlled by $\Delta F_b^*=0$. Squares=0.1 mole fraction, diamonds=0.25 mole fraction, triangles=0.5 mole fraction, and circles=0.75 mole fraction. The uppermost curve corresponds to the pure octadecane liquid case, with the thicker line portion showing the regime controlled by $\Delta F=0$ on complete crystallization.

an increase in T_c is possible for crystallization from sufficiently concentrated solutions at the smallest $|R|$ values, because the critical nucleus size is then sufficiently large compared to the substrate size, that its growth is associated with a decrease in the interfacial area, and hence the interfacial energy of the system. This superheating behavior may be accessible for systems that show surface freezing at planar interfaces, although this phenomenon is expected to be frustrated in these highly curved systems. Experiments on crystallization from long chain alkane solutions dispersed in microemulsions are in progress to investigate this.

V. DISCUSSION

Our model is undoubtedly simplistic and could be improved by, among others, considering the effects of equilibrium fluctuations,[8] which become increasingly important as the confinement size decreases, incorporating dynamical nucleation theory[29,30] and the effects of surface stress,[22,60] adding an exponential term to account for short-range interactions between the nucleus and interface,[4–6,61] including a finite length interfacial region, and removing the assumptions that the phases are incompressible and the molecular volumes of the parent and daughter phases are the same.[27] However, the inclusion of these effects will inevitably prevent a simple analytical formulation for the onset crystallization temperature. This would hinder our main aim of a readily accessible comparison of our model with both experimental and simulation data, and unmodified CNT.

Furthermore, our approach, though simplistic, does show effectively that for the smallest confinement volumes, crystallization is limited by the amount of crystallizing material, rather than the magnitude of the energy barrier, due to the supply of crystallizable molecules being depletable before $\Delta F\leq 0$. We expect this to be universally true for crystallization, and not an artifact of our model. This is readily apparent from the following. For homogeneous nucleation from the melt, decreasing the size of the confining volume at constant supersaturation does not directly affect the size of the energy barrier ΔF^*, and so as $|R|$ decreases there must always be a limiting size below which the phase transformation must be determined by the condition $\Delta F=0$ so that the new phase can attain a size r_0. This point is readily identifiable for melt crystallization in microemulsions, as the value of T_c will decrease from its previously (near) invariant value. Then, for heterogeneous nucleation if θ is approximately constant, or decreasing with $|R|$, the nucleation barrier will decrease (if our theory is applicable) and hence T_c, r^*, and r_0 will increase, and a limiting size R_{min} must always be attained. Conversely, if the energy barrier for heterogeneous crystallization increases due to, e.g., θ increasing[62] as $|R|$ decreases, then T_c, r^*, and r_0 will tend to decrease. However, the decrease in θ and T_c can only continue up to the homogeneous limit, and thereafter homogeneous nucleation again ensures that a limiting R_{min} will occur as $|R|$ decreases. For crystallization from solution in confined volumes, the value of $|R_{\text{min}}|$ will necessarily increase from the melt case, see Fig. 8. This is because the number density of the crystallizing material is reduced by the presence of the solvent and so the limiting scarcity of crystallizing material that imposes the R_{min} condition must arise at larger confinement sizes.

There is a wealth of experimental data showing an inverse, or close to inverse, relationship between the supercooling and confinement radius for melting and

crystallization.[2,3] Given that our onset crystallization temperatures for crystallization from the melt and from concentrated solutions both above and below $|R_{min}|$ predicted from Eqs. (14), (17), (22), and (24) also follow this trend when $180° > \theta_c > 90°$, our model appears to be in agreement with these experimental findings. However, it is more difficult to establish precisely which data relate to confinement conditions below $|R_{min}|$. This is particularly true for crystallization in pores due to the uncertainty in (1) whether the pores were sufficiently poorly interconnected to limit the supply of crystallizing material on the timescale of nucleation, (2) the width of any surface premelting/unfreezable layers, and (3) interfacial tension, enthalpy of fusion, and contact angle values. Data for crystallization in microemulsions, though scarcer, are often easier to interpret, since the droplet size is relatively monodisperse, the width of premelting/unfreezable layers can be known reliably,[1] the supersaturation is little affected by the confinement owing to the small/negligible Laplace pressure difference across the microememulsion droplets,[45,46] and confinement can be assumed in the absence of significant interdroplet communication. The interpretation of homogeneous nucleation data for melt crystallization in microemulsions is particularly straightforward, where we would argue that the commencement of the drop-off in onset crystallization temperatures with confinement size is sufficient to locate R_{min}. Consequently, the experimental data on homogeneous nucleation of ice in AOT microemulsions suggest a $|R_{min}|$ value ~2 nm in agreement with the predictions of our model.[1] The lack of glycine crystallization in some of the microemulsions studied by Jano *et al.*[63] also suggests confining radii $<|R_{min}|$. The (near) inverse dependence of supercooling with confinement size for $\theta_c > 90°$ is of course a necessary, but not sufficient, condition for the applicability of our model. A more stringent test that crystallization is occurring in confinement radii below $|R_{min}|$ would be the lack of hysteresis between melting and crystallization. Unfortunately, this hypothesis could not be tested in our microemulsion experiments, since the ice crystallization caused macroscopic phase separation of the oil and ice. However, the absence of hysteresis in sufficiently small pores has previously been reported by Morishige and Kawano,[64] and their data are well fitted to our model below $|R_{min}|$, see Fig. 8 in their paper. The disappearance of hysteresis for lead particles below $|R| \sim 2.5$ nm embedded in an alumina matrix has also been reported.[65] A further test for $|R| \leq |R_{min}|$ would be that crystallization could be induced by providing more crystallizing material through increased interpore connectivity in mesoporous materials or increased interdroplet communication in microemulsions to allow the exchange/coalescence of droplet content. For microemulsions, this effect would be best studied in homogeneous nucleating systems so that changes in θ could be discounted. Exchange/coalescence of droplet content may be achievable by stirring, increasing the droplet concentration, or for, e.g., AOT microemulsions, by heating above the percolation temperature of 27 °C.[66] In this latter case, crystallization may then occur despite the decrease in supercooling on heating. Experiments are in progress to test this.

The remaining question is then the likely accuracy of the R_{min}, r^*, and n^* values predicted from our model. For onset crystallization temperatures, the supersaturation is relatively low, and n^* will typically be approximately hundreds when $R = R_{min}$. Hence, the capillarity approach is reasonable for $|R| \sim |R_{min}|$ and above. For homogeneous nucleation from the melt, the R_{min} value will be readily determinable from the commencement of the decrease in T_c with decreasing $|R|$, and the reliability of the resulting r^* and n^* values when $|R| < |R_{min}|$ is then essentially limited only by the accuracy of R. For heterogeneous nucleation, reliable estimates of r^* and n^* are still possible when $|R| < |R_{min}|$ even if θ is not known accurately, just from the relative value of T_c-T_{eq}, and simple geometric and mass-balance considerations.

In summary, our model, though very simplistic, provides readily attainable and more reliable values for the observable onset melting and crystallization temperatures in small confined volumes than those obtained by using either the Gibbs–Thomson equation [compare Eqs. (1) and (2)] or the unmodified CNT (compare the "crystallization" and $\Delta F = 0$ curves shown in Fig. 7). Thus, it represents an improved framework for comparing classical capillarity approaches with experimental and simulation data in confined volumes without requiring any additional information. Our model also allows a simple and direct measurement of critical nucleus sizes in confined volumes, which circumvents the need to estimate interfacial tension and enthalpy of fusion values for the critical nucleus. Reliable values for the critical nucleus size for ice crystallization in AOT microemulsions have recently been found[1] by using this approach.

VI. CONCLUSIONS

In sufficiently small confining volumes, the phase transition temperature depends on the availability of crystallizing material and not the magnitude of the energy barrier. This means that for these systems, the critical nucleus size can be determined directly from the confining volume. No reliance on the Gibbs–Thomson equation and inappropriate usage of bulk interfacial tension and enthalpy of fusion values is required. We show this by using a very simple model based on an extended CNT and provide analytical expressions from which the critical nucleus size can be obtained directly from the confining volume. In our simple model, homogeneous phase transformations and phase transformations driven by thickening of pre-existing surface layers can be treated as limiting cases of the more general heterogeneous nucleation theory. The model predicts that for melt crystallization, onset crystallization temperatures are determinable from $(\Delta F^*_{hom} f(\theta_p)/kT_c) = \ln(A/J_{trans})$, provided that the new phase is not confined to a size smaller than $|R_{min}|$, where $R_{min} = 1.5r^* \cos\theta$. For sizes below $|R_{min}|$, crystallization is governed solely by the availability of crystallizing material to provide a thermodynamically feasible transition, with onset crystallization temperatures from the melt given by $T_c = T_{eq}[1 + (3v\gamma \cos\theta_c/|R|\Delta_{fus}H)]$. Analogous equations are also obtained for crystallization from solution. This model, though very simplistic, provides more accurate values for the

observable onset melting and crystallization temperatures in confined volumes than those obtained by using the Gibbs–Thomson equation or the unmodified CNT.

ACKNOWLEDGMENTS

We thank N. Clarke for helpful discussions. This work was supported by a grant from the Engineering and Physical Sciences Research Council.

APPENDIX A: PROOF THAT EQUATIONS (9) AND (11) ARE EQUIVALENT

Since

$$\cos\phi = \frac{x - \cos\theta}{y},$$

$$\cos^3(\theta+\phi) = \frac{(x\cos\theta - 1)^3}{y^3},$$

and

$$4x^3 f(\phi) = x^3\left(1 - \frac{x-\cos\theta}{y}\right)^2\left(2 + \frac{x-\cos\theta}{y}\right) = 2x^3 + \frac{2x^3(\cos\theta - x)}{y} + \frac{x^3\sin^2\theta(\cos\theta - x)}{y^3},$$

then,

$$0.5[1-\cos^3(\theta+\phi) + 4x^3 f(\phi) - 3x^2\cos\theta(1-\cos\phi)] = 0.5\left[1 - 3x^2\cos\theta + 2x^3 + \frac{2x^3(\cos\theta - x) + 3x^2\cos\theta(x-\cos\theta)}{y} - \frac{(x\cos\theta - 1)^3 - x^3\sin^2\theta(\cos\theta - x)}{y^3}\right]$$
$$= 0.5\left[1 - 3x^2\cos\theta + 2x^3 + \frac{-2x^4 + 5x^3\cos\theta - 3x^2\cos^2\theta}{y} - \frac{(x\cos\theta - 1)^3 - x^3\sin^2\theta(\cos\theta - x)}{y^3}\right].$$

However,

$$(x\cos\theta - 1)^3 = (x^2\cos^2\theta - 2x\cos\theta + 1)(x\cos\theta - 1) = (y^2 - x^2\sin^2\theta)(x\cos\theta - 1) = x\cos\theta y^2 - y^2 - x^3\sin^2\theta\cos\theta + x^2\sin^2\theta,$$

so

$$(x\cos\theta - 1)^3 - x^3\sin^2\theta(\cos\theta - x) = x\cos\theta y^2 - y^2 - x^3\sin^2\theta\cos\theta + x^2\sin^2\theta - x^3\sin^2\theta\cos\theta + x^4\sin^2\theta = x\cos\theta y^2 - y^2 + x^4\sin^2\theta - 2x^3\sin^2\theta\cos\theta + x^2\sin^2\theta = x\cos\theta y^2 - y^2 + x^2\sin^2\theta y^2.$$

Hence

$$0.5[1-\cos^3(\theta+\phi) + 4x^3 f(\phi) - 3x^2\cos\theta(1-\cos\phi)] = 0.5\left[1 - 3x^2\cos\theta + 2x^3 + \frac{-2x^4 + 5x^3\cos\theta - 3x^2\cos^2\theta - x\cos\theta + 1 - x^2\sin^2\theta}{y}\right]$$
$$= 0.5\left[1 - 3x^2\cos\theta + 2x^3 + \frac{-2x^4 + 5x^3\cos\theta - 2x^2\cos^2\theta - x\cos\theta + 1 - x^2}{y}\right]$$
$$= 0.5\left[1 - 3x^2\cos\theta + 2x^3 + \frac{y^2(1 - 2x^2 + x\cos\theta)}{y}\right]$$
$$= 0.5[1 - 3x^2\cos\theta + 2x^3 + y(1 + x\cos\theta - 2x^2)]$$ Q.E.D.

APPENDIX B

1. Extension of CNT to phase transitions induced by a reduction in interfacial energy

For crystallization on a convex substrate, dT_c/dR tends to zero as R approaches zero, and hence T_c just tends to the homogeneous T_c value. However, for the concave surface case, it is clear from Fig. 6(b) that dT_c/dR does not tend to zero for small confining substrates when the nucleation barrier becomes vanishingly small. This suggests that for substrate sizes smaller than this, $T_c > T_{eq}$. In this case, the phase transformation is driven not by the supersaturation of the parent phase but *by the reduction in interfacial energy that arises*. The reduction in interfacial energy upon nucleus growth is sufficiently large that it drives the phase transformation even though it produces the thermodynamically disfavored phase, and so $\Delta\mu$ and r^* are negative. Hence this case can be modeled for crystallization within substrates by determining θ_p values using positive x values, as R and r^* are both negative now. The melting of small particles with a surface liquid layer provides a well known example of this class of behavior, for which $T_m < T_{eq}$. In particular, the assignment of lower and upper bounds to the melting temperature reveals that $T_{eq}[1-\{(3\gamma v_l)/(|R|\Delta_{fus}H)\}] \leq T_m \leq T_{eq}[1-\{(2\gamma v_l)/(|R|\Delta_{fus}H)\}]$. Recent papers have formulated[4–6] the energy change on thickening of the surface layer by which melting can proceed. To a first approximation,[7] this energy change for melting of spherical particles with a surface liquid layer of width, $|R|-|r|$, is given by

$$\Delta F_{surface\_layer} = \frac{4}{3v_l}\pi\Delta\mu r^3(x^3-1) + 4\pi r^2\gamma(1-x^2), \quad \text{(B1)}$$

where v_l is the molecular volume of the liquid, R and $r<0$, and $x>1$ so that $|R|>|r|$. Melting of the whole particle occurs when r goes to zero, and the energy barrier for this process is given by $d\Delta F_{surface\_layer}/dr=0$, with constant R for melting of a given particle, for which $r^*=2\gamma v_l/\Delta\mu$. Substituting this r^* value into Eq. (B1) gives

$$\Delta F^*_{surface\_layer} = \frac{16\pi\gamma^3 v_l^2}{3\Delta\mu^2}(1-3x^2+2x^3). \quad \text{(B2)}$$

The predicted phase transformation temperature T_{trans} can then be found as for the nucleation case by setting $(\Delta F^*_{het}/kT_{trans}) = \ln(A/J_{trans})$. However, our Eq. (11), i.e., $\Delta F^*_{het} = (\Delta F^*_{hom}/2)\{1-3x^2\cos\theta+2x^3+y(1+x\cos\theta-2x^2)\} = \Delta F^*_{hom} f(\theta_p)$ reduces to Eq. (B2) when $\theta=0$, as then $\cos\theta=1$ and $y=1-x$. So Eq. (B2) just represents a limiting case of our nucleation Eq. (11).[67]

Figure 9 shows the ice onset melting temperatures given by Eq. (13a), i.e., $\Delta T_m^3 - \Delta T_m^2 T_{eq} + (16\pi\gamma^3 v_l^2 T_{eq}^2 f(\theta_p)/3k\Delta_{fus}H^2 \ln(A/J_{trans})) = 0$ for systems with surface liquid layers using the values of $v_l = 3.26\times10^{-29}$ m^3, $\gamma = 20$ mN m^{-1}, $\Delta_{fus}H = 4060$ J mol^{-1}, and $A/J_{trans} = 10^{18}$ cm^2 s^{-1}. It can be seen that the predicted onset melting temperatures fall between the upper and lower bound melting temperatures given by $T_{eq}[1-\{(2\gamma v_l)/(|R|\Delta_{fus}H)\}]$ and $T_{eq}[1-\{(3\gamma v_l)/(|R|\Delta_{fus}H)\}]$, for substrate sizes above a limiting value $|R_{min}|$, suggesting that for $|R|>|R_{min}|$, our extended nucleation theory can be used to predict onset melting temperatures. Furthermore, homogeneous nucleation represents the limiting case of Eq. (11) when $\theta=180°$. Homogeneous crystallization will occur for systems that melt via thickening of a surface liquid layer and so the crystallization curve for this case has been included in Fig. 9.

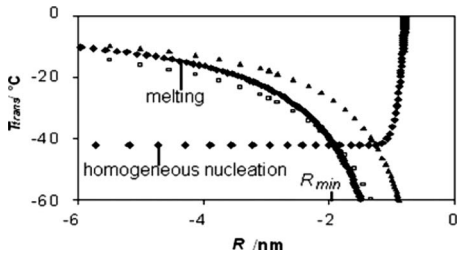

FIG. 9. The predicted ice onset melting temperature (filled diamonds) as a function of particle size for particles with surface liquid layers. Note that this melting curve falls between the upper (filled triangles) and lower (filled squares) bounds for melting, until a size R_{min} is reached, where the melting and crystallization plots meet. The homogeneous ice crystallization curve (filled diamonds) is also shown.

Figure 10 shows a schematic diagram outlining the different mechanisms for phase transitions within confined volumes. In particular, Fig. 10(a) depicts the critical nucleus for heterogeneous nucleation upon a concave substrate with $\theta > 90°$; the dashed outline represents growth of the nucleus, and this is favored for supersaturated systems since the increased volume of the thermodynamically stable phase out-

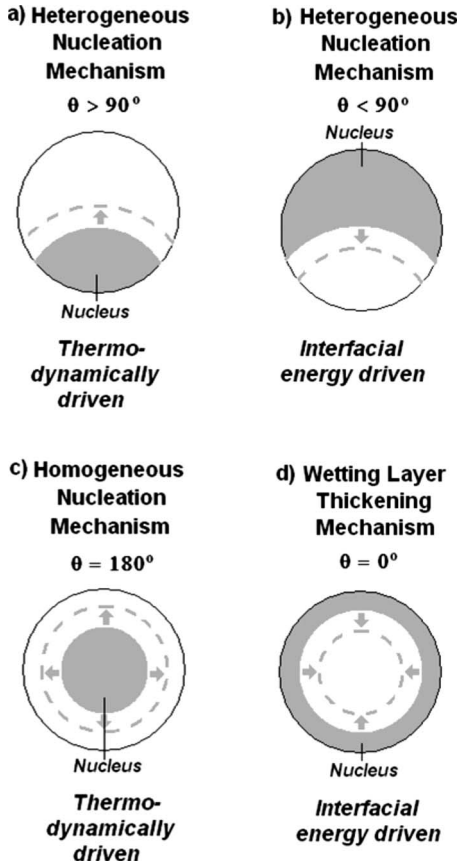

FIG. 10. Schematic diagram showing melting and melt crystallization mechanisms that can occur in confined volumes. All mechanisms can be modeled using Eqs. (11) and (13a) for confinement radii $\geq|R_{min}|$.

weighs the unfavorable increase in the interfacial energy term arising from the increased interfacial area. In contrast, Fig. 10(b) depicts the case where r^* is negative, which can occur for sufficiently small $|R|$ when $\theta < 90°$. The phase transformation is now driven by the reduction in the interfacial energy of the system. The nucleus can grow in undersaturated systems because growth, shown by the dashed line, results in a decrease in the interfacial area and hence the interfacial energy of the system, and this outweighs the unfavorable increase in volume of the thermodynamically disfavored phase. Figures 10(c) and 10(d) show the limiting cases of phase transformations occurring by homogeneous nucleation for a supersaturated system and by thickening of a pre-existing wetting layer for an undersaturated system, respectively. Again it can be seen that the nucleation mechanism requires a supersaturated system in order to compensate for the increased interfacial energy that arises from the nucleus growth shown by the dashed line, whereas if the phase transition arises from thickening of a pre-existing wetting layer, then this can occur in undersaturated systems since the interfacial energy of the system decreases with nucleus growth.

[1] J. Liu, C. E. Nicholson, and S. J. Cooper, Langmuir **23**, 7286 (2007).
[2] H. K. Christenson, J. Phys.: Condens. Matter **13**, R95 (2001).
[3] C. Alba-Simionesco, B. Coasne, G. Dosseh, G. Dudziak, K. E. Gubbins, R. Radhakrishnan, and M. Sliwinska-Bartkowiak, J. Phys.: Condens. Matter **18**, R15 (2006).
[4] R. Vanfleet and J. M. Mochel, Surf. Sci. **341**, 40 (1995).
[5] R. Denoyel and R. J. M. Pellenq, Langmuir **18**, 2710 (2002).
[6] O. Petrov and I. Furó, Phys. Rev. E **73**, 011608 (2006).
[7] The first approximation assumes that the phases are incompressible and so surface stress and surface free energy per unit area are equivalent, and that there is no volume change on phase transformation.
[8] See D. Reguera, R. K. Bowles, Y. Djikaev, and H. Reiss, J. Chem. Phys. **118**, 340 (2003). The true thermodynamic definition of the melting point of the cluster with a surface molten layer remains that given by the Gibbs–Thomson equation, however, as this defines the cluster size for which the chemical potentials of the solid and molten clusters are the same.
[9] P. R. Couchman and W. A. Jesser, Nature (London) **269**, 481 (1977).
[10] M. Volmer and A. Weber, Z. Phys. Chem. **119**, 277 (1926).
[11] R. Becker and W. Döring, Ann. Phys. **24**, 719 (1935).
[12] A. Laaksonen, V. Talanquer, and D. W. Oxtoby, Annu. Rev. Phys. Chem. **46**, 489 (1995).
[13] D. Kashchiev, J. Chem. Phys. **76**, 5098 (1982).
[14] D. W. Oxtoby and D. Kashchiev, J. Chem. Phys. **100**, 7665 (1994).
[15] R. K. Bowles, D. Reguera, Y. Djikaev, and H. Reiss, J. Chem. Phys. **115**, 1853 (2001); R. K. Bowles, D. Reguera, Y. Djikaev, and H. Reiss, J. Chem. Phys. **116**, 2330 (2002).
[16] E. Ruckenstein and Y. S. Djikaev, Adv. Colloid Interface Sci. **118**, 51 (2005).
[17] R. Evans, Adv. Phys. **28**, 143 (1979).
[18] D. W. Oxtoby and R. Evans, J. Chem. Phys. **89**, 7521 (1988).
[19] X. C. Zeng and D. W. Oxtoby, J. Chem. Phys. **94**, 4472 (1991).
[20] J. Wedekind, J. Wolk, D. Reguera, and R. Strey, J. Chem. Phys. **127**, 154515 (2007).
[21] J. Wedekind and D. Reguera, J. Chem. Phys. **127**, 154516 (2007).
[22] A. Cacciuto, S. Auer, and D. Frenkel, Phys. Rev. Lett. **93**, 166105 (2004).
[23] E. Mendez-Villuendas and R. K. Bowles, Phys. Rev. Lett. **98**, 185503 (2007).
[24] N. H. Fletcher, J. Chem. Phys. **29**, 572 (1958).
[25] M. J. Jamieson, C. E. Nicholson, and S. J. Cooper, Cryst. Growth Des. **5**, 451 (2005).
[26] D. Xu and W. L. Johnson, Phys. Rev. B **72**, 052101 (2005).
[27] D. Kashchiev and G. M. van Rosmalen, J. Colloid Interface Sci. **169**, 214 (1995).
[28] P. Hartman, in *Crystal Growth: An Introduction*, edited by P. Hartman (North-Holland, Amsterdam, 1973), p. 358.
[29] D. Reguera and H. Reiss, J. Phys. Chem. B **108**, 19831 (2004).
[30] G. K. Schenter, S. M. Kathmann, and B. C. Garrett, Phys. Rev. Lett. **82**, 3484 (1999).
[31] A. S. Shirinyan and M. Wautelet, Mater. Sci. Eng., C **26**, 735 (2006).
[32] See, e.g., J. G. Dash, Contemp. Phys. **43**, 427 (2002); J. G. Dash, A. W. Rempei, and J. S. Wettlaufer, Rev. Mod. Phys. **78**, 695 (2006), and references therein.
[33] R. R. Netz and D. Andelman, Phys. Rev. E **55**, 687 (1997).
[34] A. O. Parry, C. Rascon, and L. Morgan, J. Chem. Phys. **124**, 151101 (2006).
[35] M. C. Stewart and R. Evans, Phys. Rev. E **71**, 011602 (2005).
[36] F. O. Koenig, J. Chem. Phys. **18**, 449 (1950).
[37] V. G. Baidakov, G. Sh. Boltachev, and G. C. Chernykh, Phys. Rev. E **70**, 011603 (2004).
[38] H. M. Lu and Q. Jiang, Langmuir **21**, 779 (2005).
[39] Y. A. Lei, T. Bykov, S. Yoo, and X. C. Zeng, J. Am. Chem. Soc. **127**, 15346 (2005).
[40] E. M. Blokhuis and J. Kuipers, J. Chem. Phys. **126**, 054702 (2007).
[41] H. Reiss, P. Mirabel, and R. L. Whetton, J. Phys. Chem. **92**, 7241 (1988).
[42] R. S. Berry and B. M. Smirnov, J. Chem. Phys. **114**, 6816 (2001).
[43] R. Lovett, Rep. Prog. Phys. **70**, 195 (2007).
[44] For a summary of classical nucleation theory see, e.g., R. A. Sigsbee and G. M. Pound, Adv. Colloid Interface Sci. **1**, 335 (1967).
[45] A. Sanfeld, K. Sefiane, D. Benielli, and A. Steinchen, Adv. Colloid Interface Sci. **86**, 153 (2000).
[46] S. Ljunggren and J. C. Eriksson, Langmuir **8**, 1300 (1992).
[47] The condition that the substrate must traverse the homogeneous critical nucleus surface is always met for the concave surface case, since the maximum ΔF^*_{het} condition necessarily occurs before $(\theta+\phi)<0$. For the convex surface case, the critical nucleus completely encases the substrate if the homogeneous critical nucleus surface is not crossed, and then Eq. (11) for ΔF^*_{het} is no longer valid. Instead ΔF^*_{het} increases to $\Delta F^*_{\text{het}} = 4\pi\{\gamma(r^{*2}-R^2\cos\theta)-(\Delta\mu(r^{*3}-R^3)/3v_c)\}$ which tends to ΔF^*_{hom} as x tends to 0, and thus crystallization can only proceed at a lower temperature.
[48] H. R. Pruppacher, J. Atmos. Sci. **52**, 1924 (1995).
[49] L. S. Bartell, Annu. Rev. Phys. Chem. **49**, 43 (1998).
[50] R. J. Speedy, J. Phys. Chem. **91**, 3354 (1987).
[51] ΔF^*_{het} has a far greater temperature dependence than the pre-exponential factor, A, so we can typically treat the latter as a constant with little loss in accuracy, particularly if the temperature range of interest is relatively narrow. In addition, the rapid increase in the nucleation rate with supercooling above the Ostwald metastability limit ensures that we can set the nucleation rate at T_c as a suitable detection limit without incurring any significant error.
[52] Note that θ_p is undefined for the interfacial energy driven mechanism as r^* is negative and $|\cos\theta_p| = |x-y| > 1$, although of course $f(\theta_p)$ still gives a measure of ΔT_{trans}. Instead the angle $\theta_{p\_1} = \arccos(-x-y)$ gives a geometric measure of the magnitude of ΔT_{trans}.
[53] B. V. Enustun, B. W. Gunnick, and T. Demirel, J. Colloid Interface Sci. **134**, 264 (1990).
[54] R. Radhakrishnan, K. E. Gubbins, A. Watanabe, and K. Kaneko, J. Chem. Phys. **111**, 9058 (1999).
[55] J. Yano, H. Furedi-Milhofer, E. Watchel, and N. Garti, Langmuir **16**, 9996 (2000).
[56] H. Kraack, E. B. Sirota, and M. Deutsch, J. Chem. Phys. **112**, 6873 (2000).
[57] E. B. Sirota, J. Chem. Phys. **112**, 492 (2000).
[58] E. B. Sirota and A. B. Herhold, Science **283**, 529 (1999).
[59] B. Xie, H. Shi, S. Jiang, Y. Zhao, C. C. Han, D. Xu, and D. Wang, J. Phys. Chem. B **110**, 14279 (2006).
[60] A. Cacciuto and D. Frenkel, J. Phys. Chem. B **109**, 6587 (2005).
[61] R. Lipowsky, Phys. Rev. Lett. **52**, 1429 (1984).

[62] It is also possible that inaccuracies in our simple theory, e.g., the lack of inclusion of line tension effects, could also cause the free energy barrier to increase.
[63] J. Yano, H. Furedi-Milhofer, E. Watchel, and N. Garti, Langmuir **16**, 10005 (2000).
[64] K. Morishige and K. Kawano, J. Chem. Phys. **110**, 4867 (1999).
[65] P. Cheyssac, R. Kofman, and R. Garrigos, Phys. Scr. **38**, 164 (1988).
[66] D. Senatra, R. Pratesi, and L. Pieraccini, J. Therm Anal. Calorim. **51**, 79 (1998).
[67] In fact, Eq. (B1) for $\Delta F_{\text{surface\_layert}}$ is also just the limiting case of our Eq. (8) when $\theta=0$ and both R and r are negative in our model, as then $\cos(\theta+\phi)$ and $\cos(\phi)$ both equal -1 if $x>1$ and so $f(\theta+\phi)$ and $f(\phi)$ are equal to 1. Note that if $x<1$, then the solutions are not valid as $|R|<|r|$.